DTIC FILE COPY

SECURITY CLASSIFICATION OF THIS PAGE

REPORT DOCUMENTATION PAGE

Form Approved OMB No. 0704-0188

1a. REPORT SECURITY CLASSIFICATION UNCLASSIFIED	1b. RESTRICTIVE MARKINGS NONE
AD-A217 854	3. DISTRIBUTION/AVAILABILITY OF REPORT APPROVED FOR PUBLIC RELEASE; DISTRIBUTION UNLIMITED.
4. PERFORMING ORGANIZATION REPORT NUMBER(S)	5. MONITORING ORGANIZATION REPORT NUMBER(S) AFIT/CI/CIA- 89-101
6a. NAME OF PERFORMING ORGANIZATION AFIT STUDENT AT AZ St Univ 6b. OFFICE SYMBOL (If applicable)	7a. NAME OF MONITORING ORGANIZATION AFIT/CIA
6c. ADDRESS (City, State, and ZIP Code)	7b. ADDRESS (City, State, and ZIP Code) Wright-Patterson AFB OH 45433-6583
8a. NAME OF FUNDING/SPONSORING ORGANIZATION 8b. OFFICE SYMBOL (If applicable)	9. PROCUREMENT INSTRUMENT IDENTIFICATION NUMBER
8c. ADDRESS (City, State, and ZIP Code)	10. SOURCE OF FUNDING NUMBERS PROGRAM ELEMENT NO. / PROJECT NO. / TASK NO / WORK UNIT ACCESSION NO.

11. TITLE (Include Security Classification) (UNCLASSIFIED)
AN EXPERIMENTAL INVESTIGATION OF THE THERMAL CONDUCTIVITY OF POROUS ADSORBENTS

12. PERSONAL AUTHOR(S)
JOSEPH JAMES SECARY

13a. TYPE OF REPORT	13b. TIME COVERED	14. DATE OF REPORT (Year, Month, Day)	15. PAGE COUNT
THESIS/DISSERTATION	FROM _____ TO _____	1989	52

16. SUPPLEMENTARY NOTATION
APPROVED FOR PUBLIC RELEASE IAW AFR 190-1
ERNEST A. HAYGOOD, 1st Lt, USAF
Executive Officer, Civilian Institution Programs

17. COSATI CODES			18. SUBJECT TERMS (Continue on reverse if necessary and identify by block number)
FIELD	GROUP	SUB-GROUP	

19. ABSTRACT (Continue on reverse if necessary and identify by block number)

DTIC ELECTE FEB 12 1990 S D

20. DISTRIBUTION/AVAILABILITY OF ABSTRACT ☒ UNCLASSIFIED/UNLIMITED ☐ SAME AS RPT. ☐ DTIC USERS	21. ABSTRACT SECURITY CLASSIFICATION UNCLASSIFIED
22a. NAME OF RESPONSIBLE INDIVIDUAL ERNEST A. HAYGOOD, 1st Lt, USAF	22b. TELEPHONE (Include Area Code) (513) 255-2259 / 22c. OFFICE SYMBOL AFIT/CI

DD Form 1473, JUN 86 *Previous editions are obsolete.* SECURITY CLASSIFICATION OF THIS PAGE

AFIT/CI "OVERPRINT"

89-101

Capt Ujcik,

I'm providing you with a copy of my thesis, two copies of my abstact and two copies of my sources along with the following information as per AFIT 53-1 chapter 7.

AUTHOR: Joseph James Secary

TITLE: AN EXPERIMENTAL INVESTIGATION OF THE THERMAL CONDUCTIVITY OF POROUS ADSORBENTS

RANK: 2ndLt

BRANCH: U.S.A.F.

DATE: 1989

NUMBER OF PAGES: 61

DEGREE: Master of Science

INSTITUTION: Arizona State University

Accesion For	
NTIS CRA&I	☑
DTIC TAB	☐
Unannounced	☐
Justification	
By	
Distribution /	
Availability Codes	
Dist	Avail and / or Special
A-1	

DTIC COPY INSPECTED 8

90 02 12 038

AN EXPERIMENTAL INVESTIGATION

OF THE

THERMAL CONDUCTIVITY OF POROUS ADSORBENTS

by

Joseph James Secary

A Thesis Presented in Partial Fulfillment
of the Requirements for the Degree
Master of Science

ARIZONA STATE UNIVERSITY

May 1989

AN EXPERIMENTAL INVESTIGATION

OF THE

THERMAL CONDUCTIVITY OF POROUS ADSORBENTS

by

Joseph James Secary

has been approved

May 1989

APPROVED:

_____, Chairperson

_____

_____

Supervisory Committee

ACCEPTED:

_____

Department Chairperson

_____

Dean, Graduate College

ABSTRACT

The thermal conductivities of Praseodymium-Cerium-Oxide (PCO) and Saran Carbon have been experimentally investigated using a steady-state heat transfer technique. The investigated substances are used as adsorbents in adsorption compressors being developed for spaceborne refrigeration applications. The objectives of the investigation were to determine the thermal conductivities and establish their temperature dependency. Data were collected for the PCO over a temperature range of 300°C to 600°C, and 0°C to 200°C for the Saran Carbon. The thermal conductivities were found to have a strong temperature dependency. In particular, the results for the PCO showed a temperature dependency indicative of some thermal radiation effects.

Key words: Thermal conductivity, adsorbents, space missions, space technology, compressors, praseodymium compounds, Thermal insulation. (EMR)

ACKNOWLEDGMENTS

I wish to acknowledge my indebtedness to my advisor Dr. T. W. Tong, who gave me the opportunity to do experimental work.

I am grateful to my colleagues Sanjeev Sathe and Sharat Chandra for their active support during this work. I also wish to thank my wife and daughter for their understanding and moral support during the long hours spent on this project.

TABLE OF CONTENTS

LIST OF TABLES

LIST OF FIGURES

NOMENCLATURE

A	=Area perpendicular to the energy transfer
ΔA	=Uncertainty in A
count	=Number of pulses to inner heater in Δt
Δcount	=Uncertainty in count
D_i	=Outer diameter of inner heater
D_o	=Outer diameter of the side guard heater
k	=Thermal conductivity
k_l	=Thermal conductivity of interstitial fluid
k_s	=Thermal conductivity of solid carbon
k_{ss}	=Thermal conductivity of stainless steel
Δk_{ss}	=Uncertainty in k_{ss}
Q	=Energy transferred across the sample
R	=Resistance of inner heater
ΔR	=Uncertainty in R
ΔT	=Temperature difference between hot and cold surfaces of the sample ($T_h - T_c$)
Δt	=Time interval in seconds
$\Delta(\Delta t)$	=Uncertainty in Δt
T_c	=Temperature of cold plate
ΔT_c	=Uncertainty in T_c
T_{car}	=Temperature difference in Saran Carbon
T_h	=Temperature of the hot plate
ΔT_h	=Uncertainty in T_h
T_{mean}	=Arithmetic mean temperature ($(T_h + T_c)/2$)

ΔT_{ss} =Temperature difference in the stainless-steel column

Δx =Sample thickness

$\Delta(\Delta x)$ =Uncertainty in Δx

Δx_{car} =Distance between thermocouple locations in Saran Carbon

Δx_{ss} =Distance between thermocouple locations in stainless stee column

Ve =R.m.s. voltage drop across inner heater

ΔVe =Uncertainty in Ve

CHAPTER 1

INTRODUCTION

In space, a refrigeration system is needed to provide cooling to many instruments located onboard the spacecraft. Typically, refrigeration systems have relied on mechanically driven compressors to compress the working fluid. These compressors are not advantageous for space application because they have wear-related moving parts which limit the mission duration. An alternative is to replace the mechanically driven compressors with adsorption compressors. Because of the lack of moving parts non-mechanical adsorption compressors offer a longer operating life, far exceeding mechanically driven compressors.[1]

Adsorption compressors are essentially canisters filled with a porous material that desorbs and adsorbs gases as the temperature in the canister is increased and decreased.[2] By thermally cycling a number of canisters filled with a porous adsorbent, it is possible to provide a flow of high pressure gas for the refrigeration system.

Currently, the Jet Propulsion Laboratory (JPL) in Pasadena, California is developing a laboratory model of an absorption cryocooler system[1,3] which uses Saran Carbon, and Praseodymium-Cerium-Oxide (PCO) for the porous adsorbent. In conjuction with JPL, numerical studies are being

conducted by Sathe and Tong to better understand the heat and fluid flow characteristics inside the porous medium.[4] At the present time, these studies use an assumed value for the thermal conductivity of the Saran Carbon and PCO due to lack of data. To generate more realistic numerical values the assumed values should be replaced by experimentally obtained values.

Fourier's law of heat conduction was used in obtaining the thermal conductivities of the porous material. When applied to a planar medium as depicted in Figure 1, Fourier's law yields the following relationship

$$k = Q\Delta x/A\Delta T \qquad (1)$$

where Q is the energy transferred across the sample, Δx is the sample thickness, A is the area perpendicular to the energy transfer, and ΔT is the temperature difference between the hot and cold surfaces of the sample, i.e. $T_h - T_c$. The above equation is valid only for the case of one-dimensional, steady-state energy transfer, and a non-temperature dependent (constant) thermal conductivity. Although the thermal conductivity of materials is usually temperature dependent, the dependency effect is minimized if ΔT is small. The thermal conductivity can be determined once the variables on the right-hand side of the equation are measured.

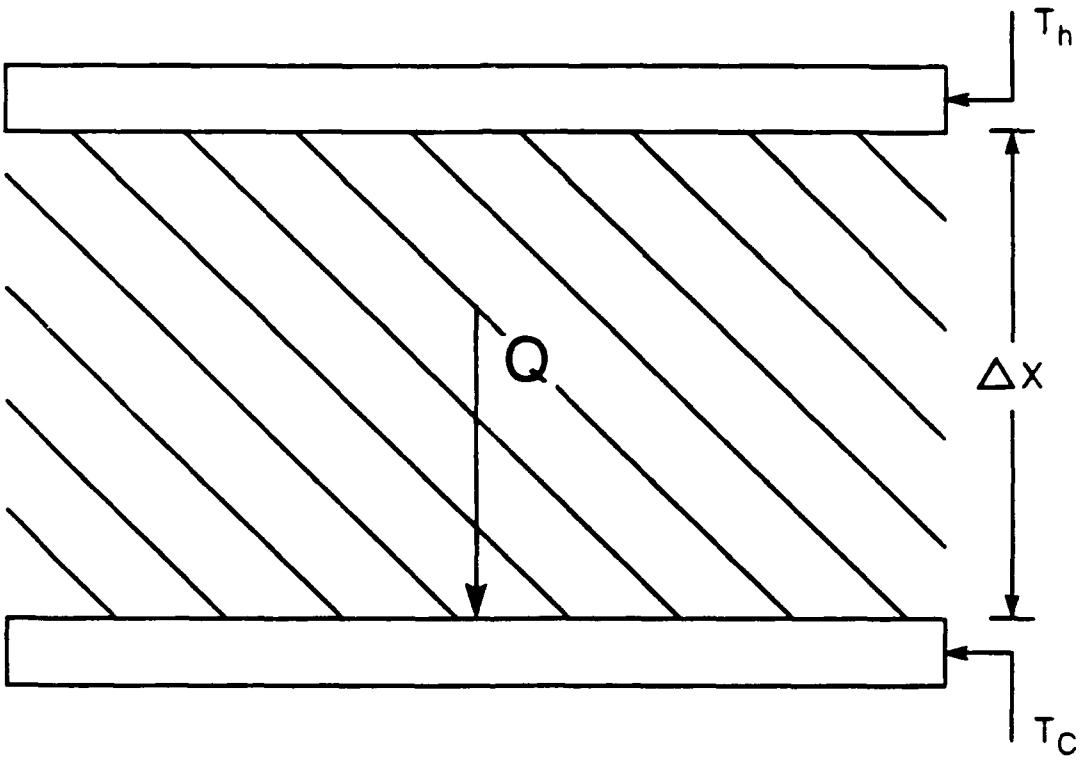

Fig. 1 One-dimensional heat conduction through a planar medium

CHAPTER 2

EXPERIMENTAL METHOD

As mentioned ealier, the two types of porous material used in the adsorption compressors of interest are PCO and Saran Carbon. To determine the thermal conductivities of these materials, two different test sections were designed and built. Two test sections were needed because of the composition of the available porous material. The PCO was in powder form while the Saran Carbon was in the form of a rigid rod. Both test sections produce steady-state, one-dimensional heat transfer across the material of interest.

2.1 Heat Transfer Considerations for the Design of the PCO Test Apparatus

To measure the thermal conductivity of the PCO a circular guarded-hot-plate apparatus[5,6] was designed and built. Figure 2 shows the basic construction of a guarded-hot-plate apparatus. The bottom heater consists of two sections, the inner or test section, and a side guard section. To minimize heat loss in the lateral direction from the test section, the temperature of the outer hot plate is matched with that of the inner hot plate by appropriately adjusting the side guard heater. Similarly, the rear guard heater, the top plate, and the insulation are used to reduce heat transfer in the upward direction. This

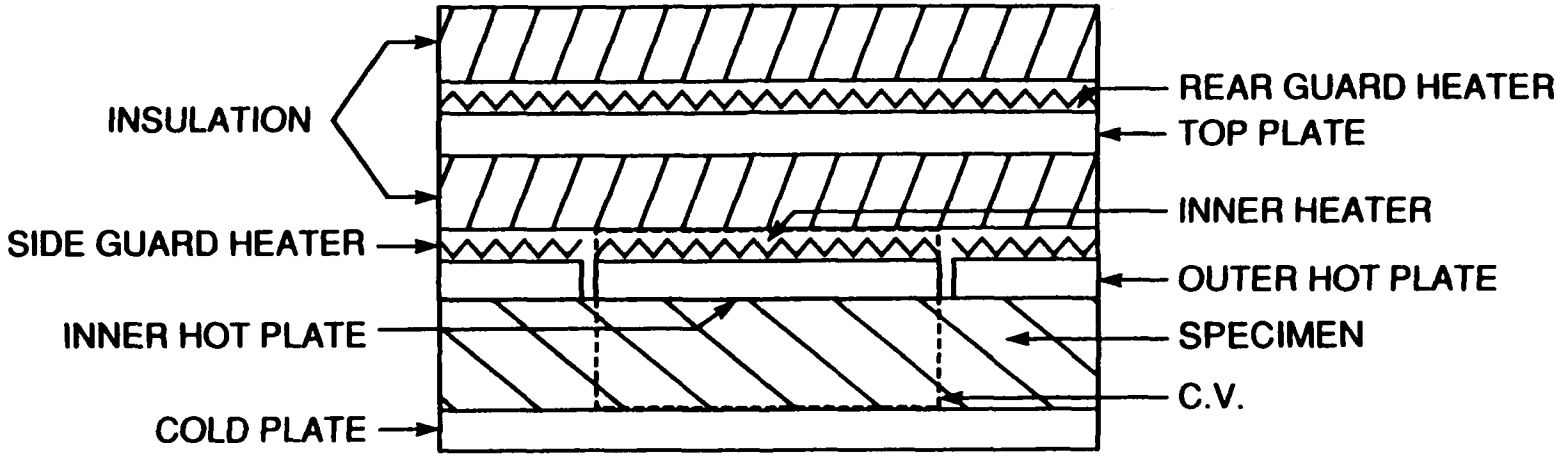

Fig. 2 Cross-sectional view of the guarded-hot-plate apparatus

ensures that heat transfer from the test section can be regarded as downward and one-dimensional through the control volume (C.V.). To arrive at the dimensions of the apparatus, a heat transfer analysis was performed. The purpose was to determine the dimensions of the different sections so that heat transfer through the control volume could in fact be treated as one-dimensional.

A Fortran algorithm SIMPLE was used to thermally model the idealized guarded-hot-plate apparatus, as shown in Figure 3. Adiabatic condition was assumed for the surface above the heaters. The heaters were modeled as Inconel (0.64 cm thick) discs with uniform heat generation. The inner and outer hot plates were assumed to be copper (0.64 cm thick). The support wall (0.32 cm thick) and the reference plate (0.64 cm thick) were taken as stainless-steel. SIMPLE is a finite-difference algorithm[7] which can be used to solve for the steady-state temperature distribution in two-dimensional objects. Calculations can be performed using one of three different coordinate systems: r-x, x-y, and r-θ. The coordinate system used in this study was r-x.

The temperature distribution calculated in the apparatus can be used to provide an energy balance on the control volume shown in Figure 3. Since the amount of energy passing through the sides and bottom of the control volume can be calculated the energy loss then becomes a

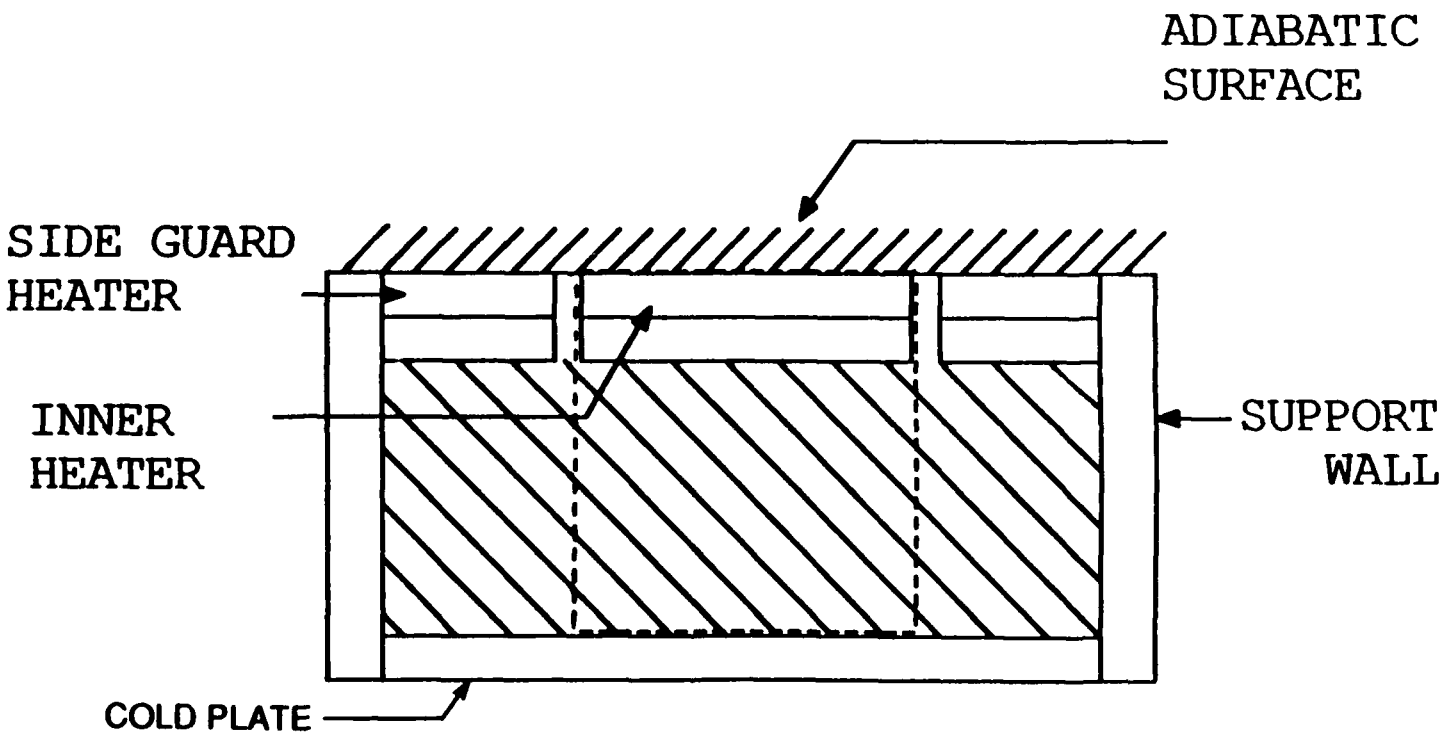

Fig. 3 Cross-sectional view of the idealized guarded -hot-plate apparatus

known quantity. The energy loss on a percentage basis is defined as the amount of energy transferred through the sides of the control volume divided by the energy generated in the inner heater. Thus, it is an indicator of how good the one-dimensional heat flow assumption is for the experiment. An acceptable energy loss of 5 percent or less was used as a constraint on the design process.

Figure 4 shows the relationship between the percent energy loss and the ratio of D_o to D_i for different sample thicknesses. In this case, D_o is the outer diameter of the side guard heater, and D_i is the outer diameter of the inner heater. The results are for k = 0.05 W/m*C, which should yield a conservative estimate of the energy loss since it is rather small. As indicated in the figure, the energy loss on a percentage basis decreases as D_o/D_i increases for different sample thicknesses. Also, thicker samples result in higher energy loss. The figure was used to determine the dimensions of the guarded-hot-plate apparatus for the PCO experiment. This was accomplished by finding the region on Figure 4 where the energy loss would be 5 percent or less, and then picking a point somewhere in the region. In this experiment, a sample thickness of 0.64 cm and a D_o/D_i ratio of 1.45 was selected to meet the energy loss constraint. According to Figure 4, the percent energy loss would be 4.6 percent.

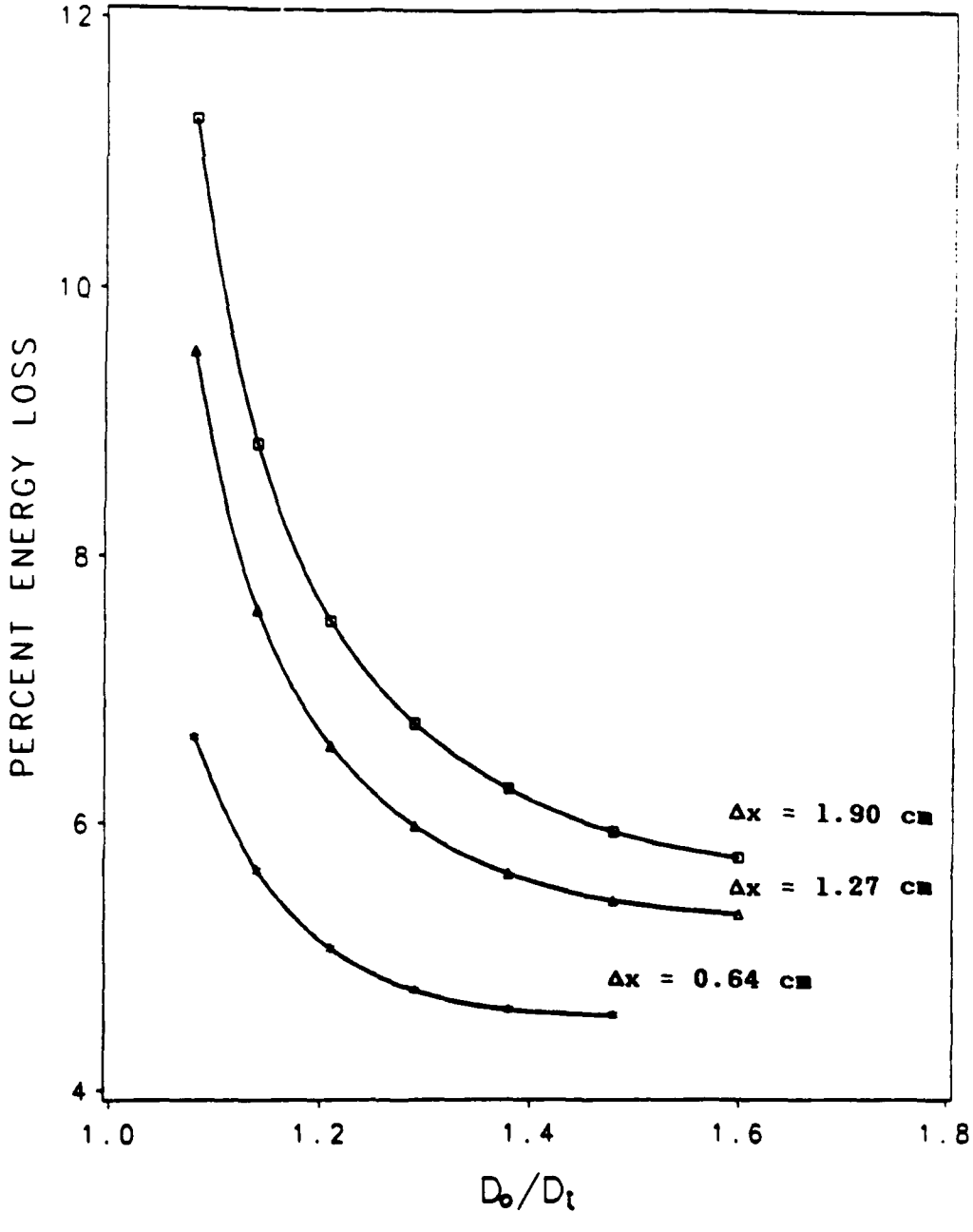

Fig. 4 Percent energy loss against D_o/D_i for k = 0.05 W/m°C

Figure 5 shows the percent energy loss as a function of thermal conductivity for the dimensions chosen above. As indicated in the figure, the energy loss decreases exponentially as the thermal conductivity increases. Therefore, if the actual thermal conductivity of the PCO is greater than 0.05 W/m°C, the percent energy loss would be less than 4.6 percent.

2.2 PCO Experimental Apparatus

The PCO experimental apparatus, which can be seen in Figure 6, is suitable for thermal conductivity measurements on materials up to temperatures of 700°C. The vacuum chamber allows for measurements under vacuum conditions in order to eliminate gaseous heat conduction. The dimensions of the apparatus are as indicated in the figure. The wall that encloses the PCO is a stainless steel tube with holes drilled through the sides to facilate evacuation of the PCO. The PCO experimental apparatus was placed inside a vacuum chamber by bolting the reference plate to a flange located at the bottom of the chamber.

The hot plate sections were fabricated from 0.64 cm thick copper plate and the reference plate (cold plate) from 1.27 cm stainless-steel. An inner heater and guard heater were installed between the bottom copper plates and insulation. A 0.64 cm thick copper plate was placed on top of the insulation and another heater (the rear guard heater)

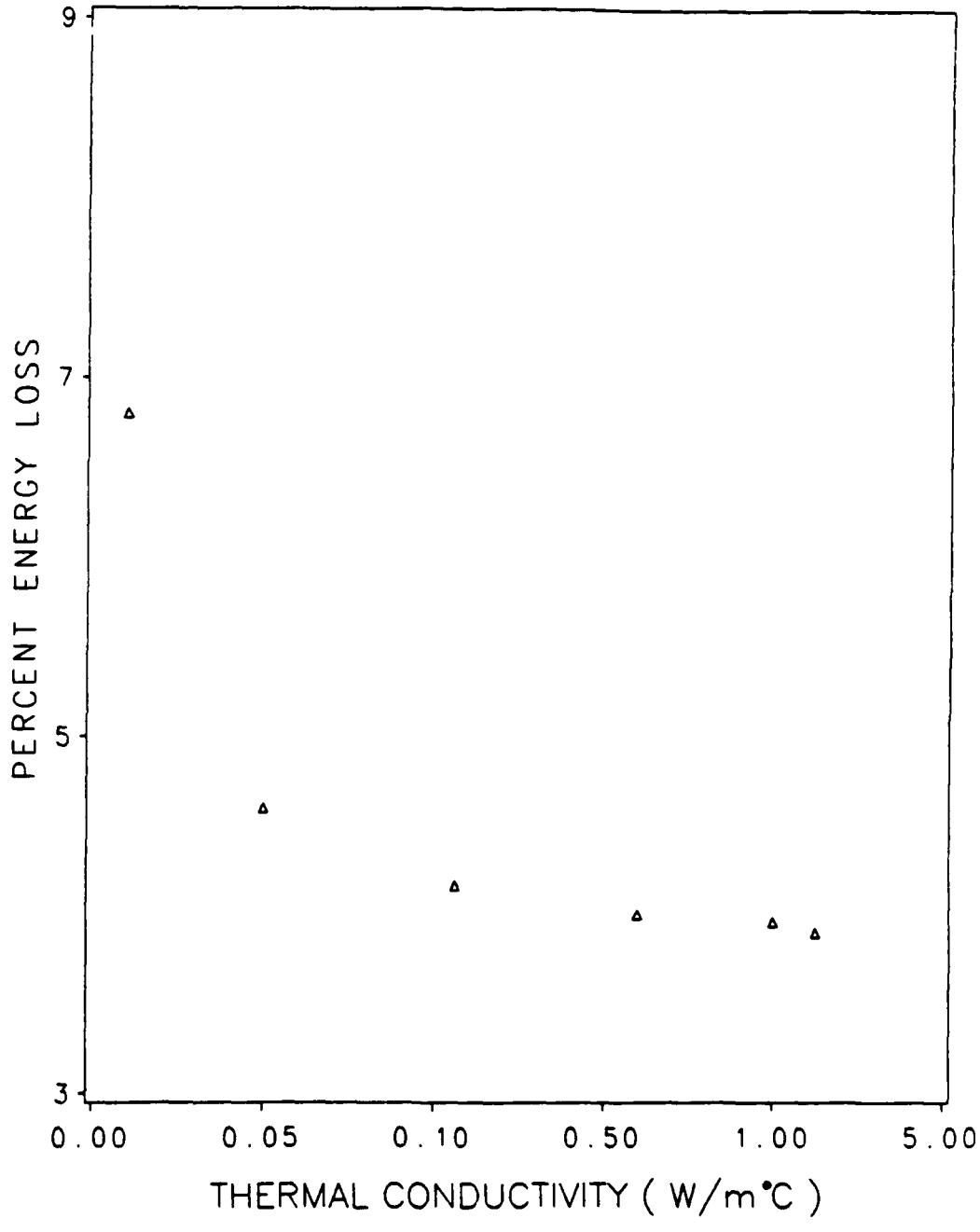

Fig. 5 Percent energy loss against thermal conductivity

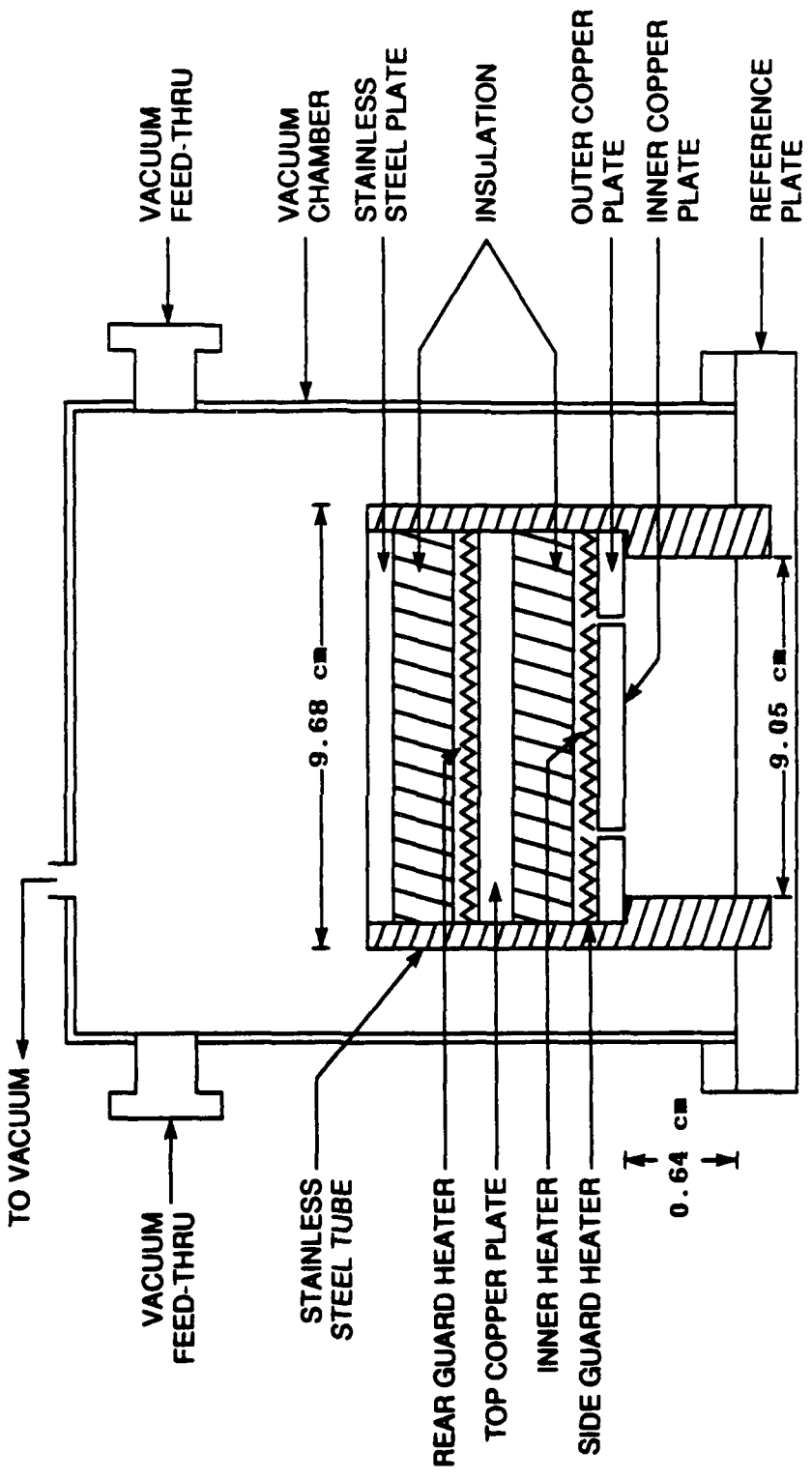

Fig. 6 PCO experimental apparatus

was placed on top of the plate. An upper piece of insulation was placed on the rear guard heater and a 0.64 cm thick stainless-steel plate was placed on top of the insulation.

Eight bare-wire Chromel-Alumel thermocouples, 0.038 cm diameter, were installed in grooves machined in the upward-face of the copper plates. The thermocouple beads were installed in small holes drilled into the ends of the grooves. The bare wires were coated with a high temperature cement (Omega CC) and placed in the grooves. This ensured good electrical isolation of the bare wires from each other as well as from the copper plates. The grooves were filled in with a highly conductive material (Steel Seal) to ensure an uniform temperature distribution throughout the plates. Figure 7 shows the locations of the thermocouples.

Two insulated Chromel-Alumel thermocouples were installed into the bottom of the reference plate at the mid-plane position. The thermocouples were held into place by retaining clips attached to the reference plate. The insulation was covered with stainless-steel braiding to protect the thermocouples from the aluminum oxide sand used in the constant temperature bed which will be dicussed later. The locations of the reference plate thermocouples can be found in Figure 8.

The temperature of the copper plates was regulated by three Digi-Sense proportional controllers (model # 2168-80).

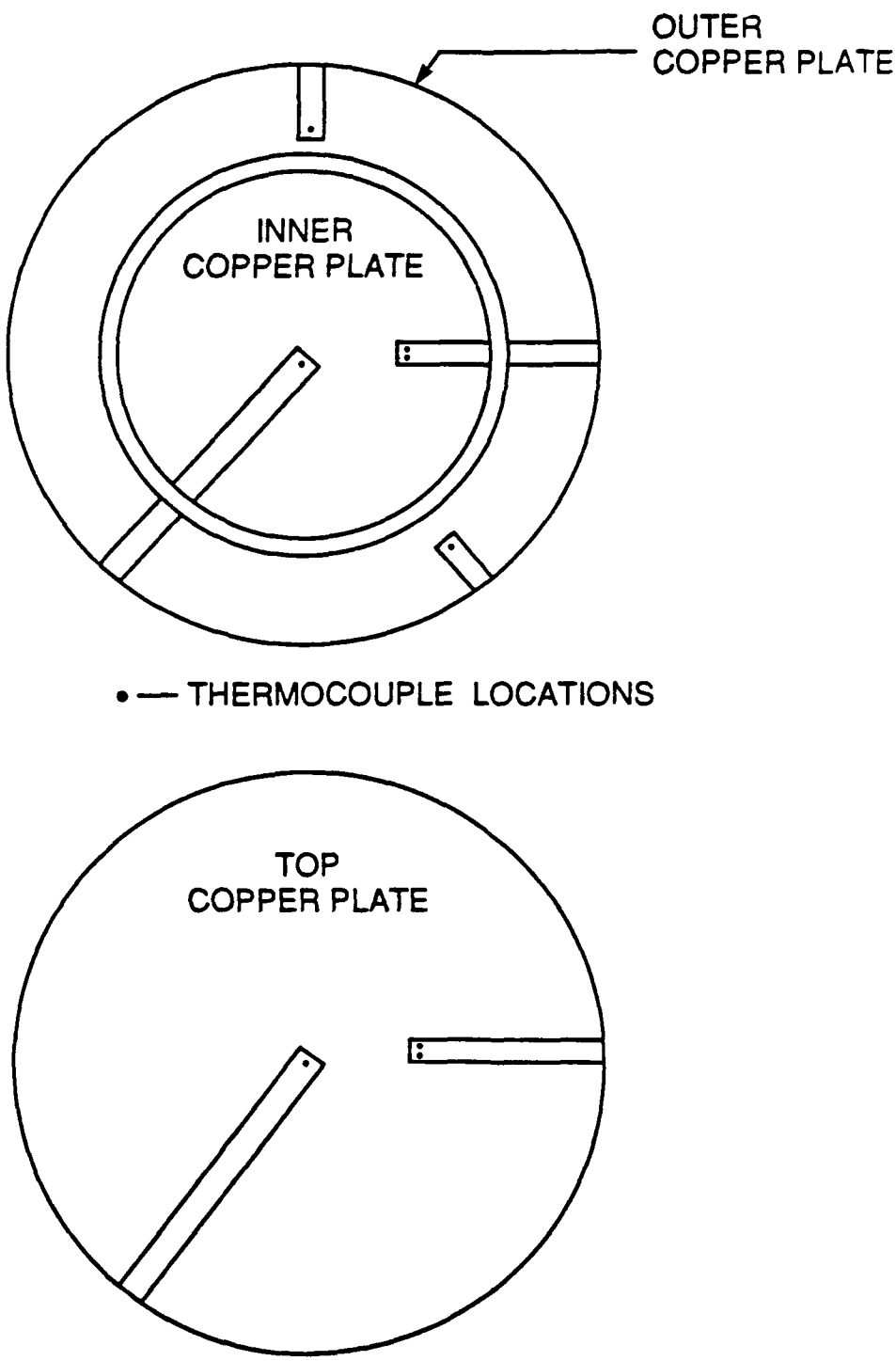

Fig. 7 A view of the upward-facing surfaces of the hot plate assembly

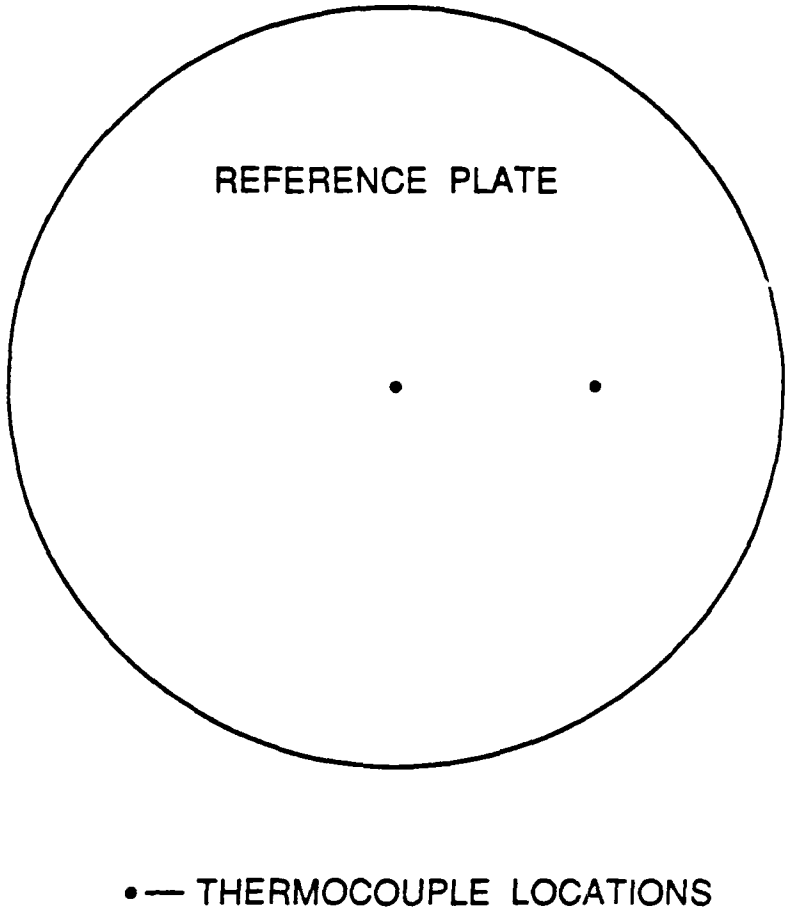

Fig. 8 A view of the downward-facing surface of the reference plate

The temperature controllers automatically controlled the temperature by regulating the electrical current into the heaters, depending upon the signal they received from the thermocouple sensors located inside the copper plates. A power pulse meter was used to measure the amount of average power delivered to the inner heater at steady-state conditions. This was done by measuring the number of pulses delivered to the inner heater in a certain time interval, and the resistance as well as the r.m.s. value of the voltage drop across the main heater (see Appendix A). The amount of average power delivered to the inner heater at steady-state corresponds to Q in equation (1).

The thermocouple and heater leads inside the chamber were connected to a vacuum feedthrough system located on the side of the chamber (see Figure 6). The feedthrough was used to insure no leakage into the chamber from the surrounding room air. The feedthrough leads were connected to a thermocouple switchbox located outside the chamber. The error introduced by the feedthrough system was determined by calibrating a thermocouple circuit with the feedthrough system installed against a thermocouple circuit without the feedthrough. Data taken at various temperatures revealed negligible error due to the feedthrough system (see Appendix B).

Figure 9 shows a schematic of the overall system used in the experiment. Because measurements with the reference

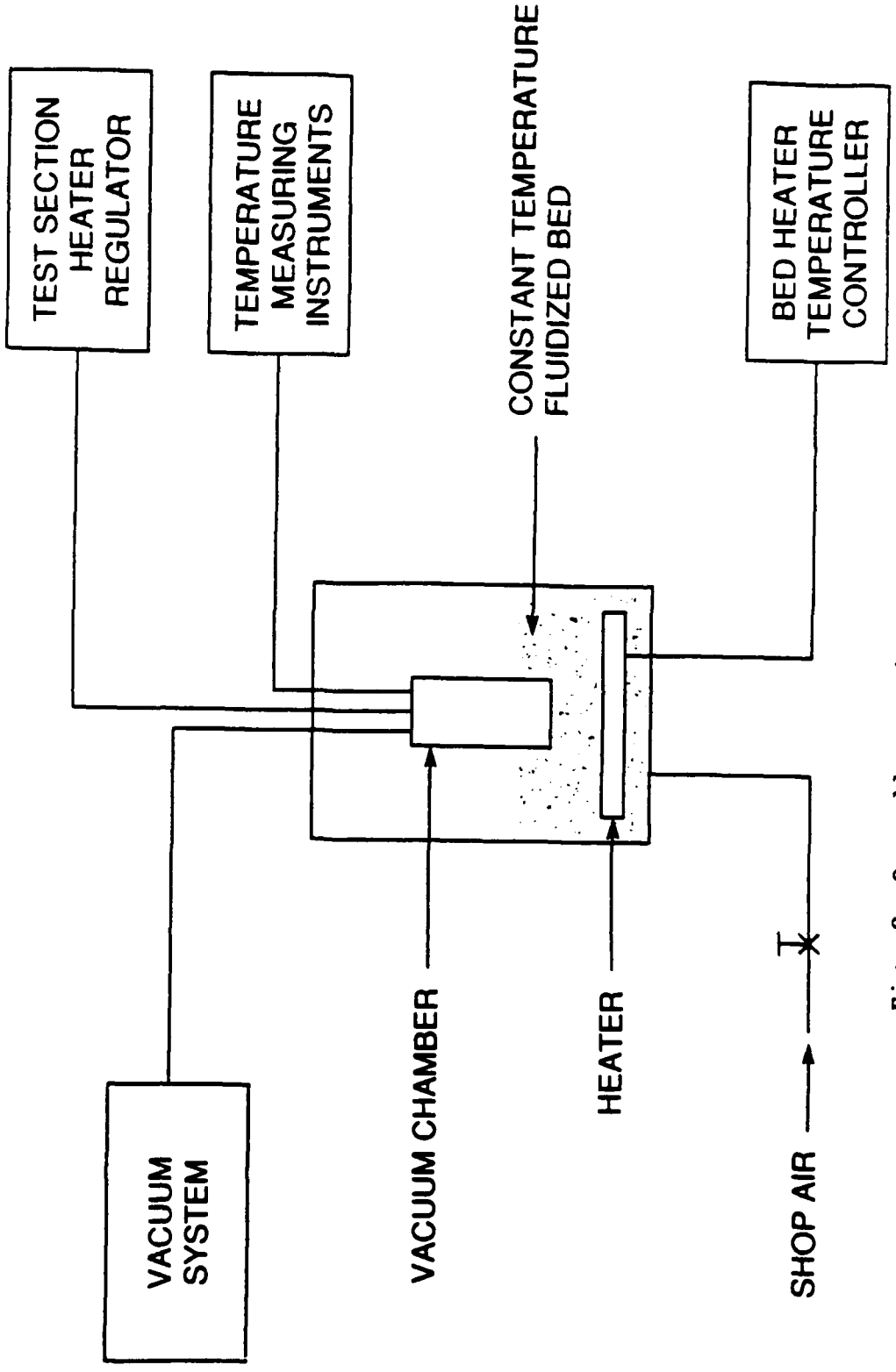

Fig. 9 Overall experimental system

plate temperature as high as 600°C were needed, a fluidized sand bed was used to control the reference plate temperature by immersing the vacuum chamber (with the reference plate attached) into the bed. The bed was capable of providing rapid heat transfer and precise temperature control of the reference plate, in the range of 50°C to 600°C. The bed heater temperature controller was used to maintain the bed temperature to within ± 0.2°C of desired setting. A FLUKE multimeter (model # 8842A) was used to collect the millivolt readings from the thermocouples installed in the experimental apparatus.

The schematic diagram in Figure 10 shows the major components of the vacuum system. The mechanical roughing pump was used to pump down the system to the pressure where the turbomolecular pump could start pumping. The turbomolecular pump was used to obtain the desired vacuum level. The thermocouple and ionization gauges were used to register the pressure in the system from atmosphere to 10^{-9} torr. A variable leak valve provided a means to control the level of vacuum inside the chamber. For the PCO powder (10 μm in diameter) a vacuum level of 1×10^{-3} torr or better was needed. This insured that the mean free path of the interstitial fluids would exceed the spacing between the PCO particles, thereby eliminating gaseous conduction.[8] For most of the experimental runs, a vacuum of better than 8×10^{-5} torr was achieved.

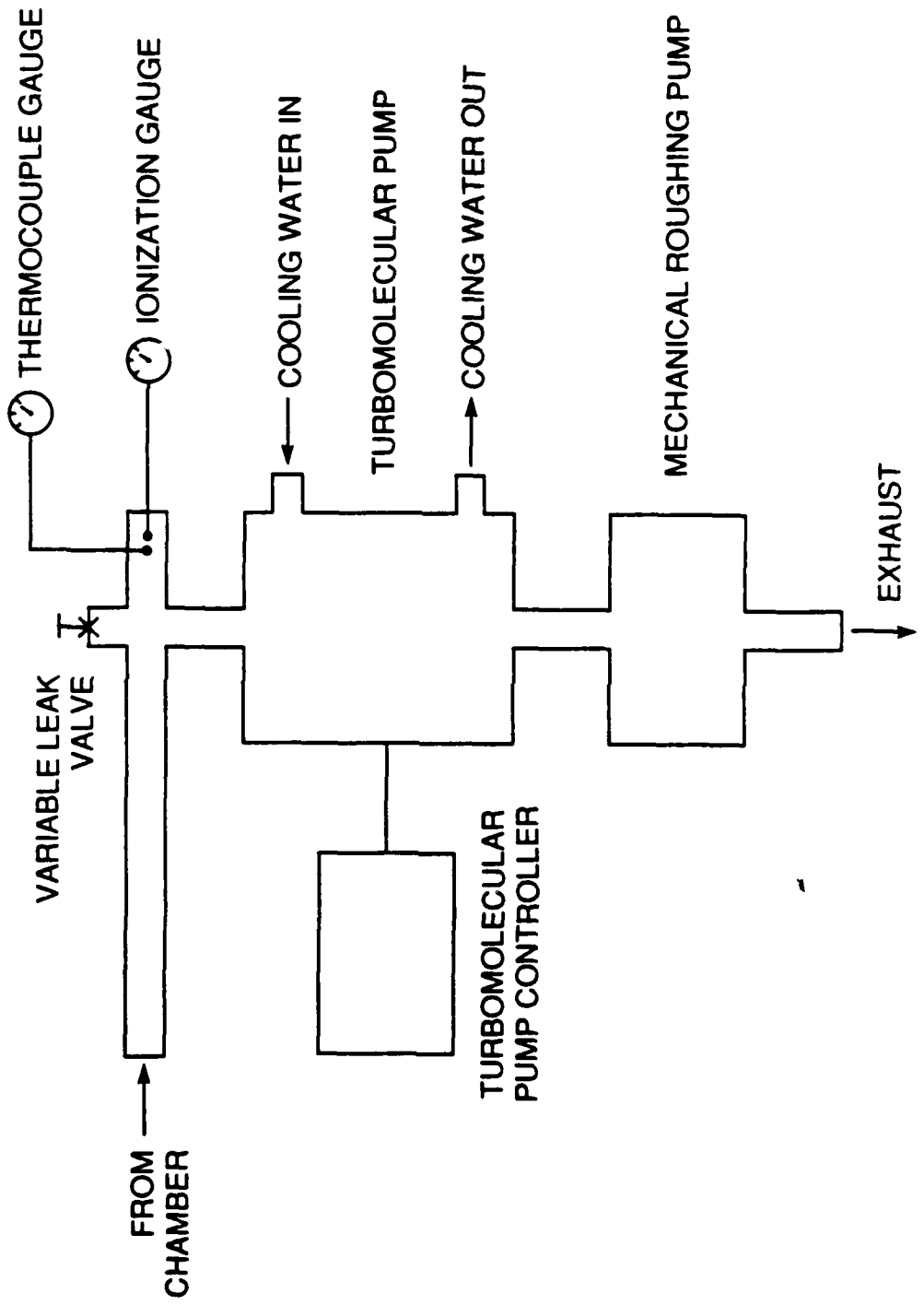

Fig. 10 Components of the vacuum system

2.3 Experimental Procedure

PCO was placed inside the apparatus between the bottom copper plates and the reference plate (see Figure 6). This was done by first attaching the stainless-steel tube to the reference plate. Then, by using a ram assembly, loose PCO powder (approximately 10 μm in diameter) was compressed, by JPL, to a depth of 0.64 cm and density of 3.5 grams/cm^3, into the bottom of the stainless-steel tube. The hot plate section was then placed on top of the PCO and the reference plate was bolted, after attaching the thermocouple and heater leads to the feedthrough system, to the vacuum chamber as explained in section 2.2.

Once the PCO apparatus had been bolted to the vacuum chamber the system was placed into the constant temperature fluidized bed. The vacuum system was turned on and the vacuum level inside the chamber reached 8×10^{-5} torr. After outgassing, all temperature controllers were set to the desired ΔT, typically around 25°C, across the top and bottom surfaces of the PCO. The level of vacuum inside the chamber was then set to a predetermined reading and data were taken at 30 minute intervals until steady-state conditions were obtained. In this experiment, steady-state conditions existed when the desired ΔT did not vary more than $\pm$ 0.5°C over a 60-min interval. The procedure was then repeated for different hot- and reference- plate temperatures. The data

collected consisted of the temperature at each thermocouple location, number of pulses to the inner heater in a time interval, and bed temperature. The thermal conductivity was then calculated using equation (1). The uncertainties in the values of the thermal conductivity ranged from ± 2.44 percent to ± 2.56 percent as given in Appendix C.

2.4 Heat Transfer Considerations for the Design of the Carbon Test Section

To measure the thermal conductivity of the Saran Carbon a different type of apparatus, based on previous designs[9,10,11], was designed and built. The basic apparatus can be seen in Figure 11. The apparatus consists of two columns with the test specimen sandwiched between them. The objective is to achieve one-dimensional heat conduction from one end of the carbon rod to the other. A heat source is attached to the top column to provide the needed heat transfer into the test specimen.

SIMPLE was used to thermally model the apparatus. This was done to determine if heat transfer in the carbon rod could be treated as one-dimensional. The same procedure as discussed before (see section 2.1) was used to determine the energy loss through the sides of the control volume shown in Figure 11. In this investigation, these losses never exceeded 1.6 percent, indicating the one-dimensional heat conduction assumption was acceptable.

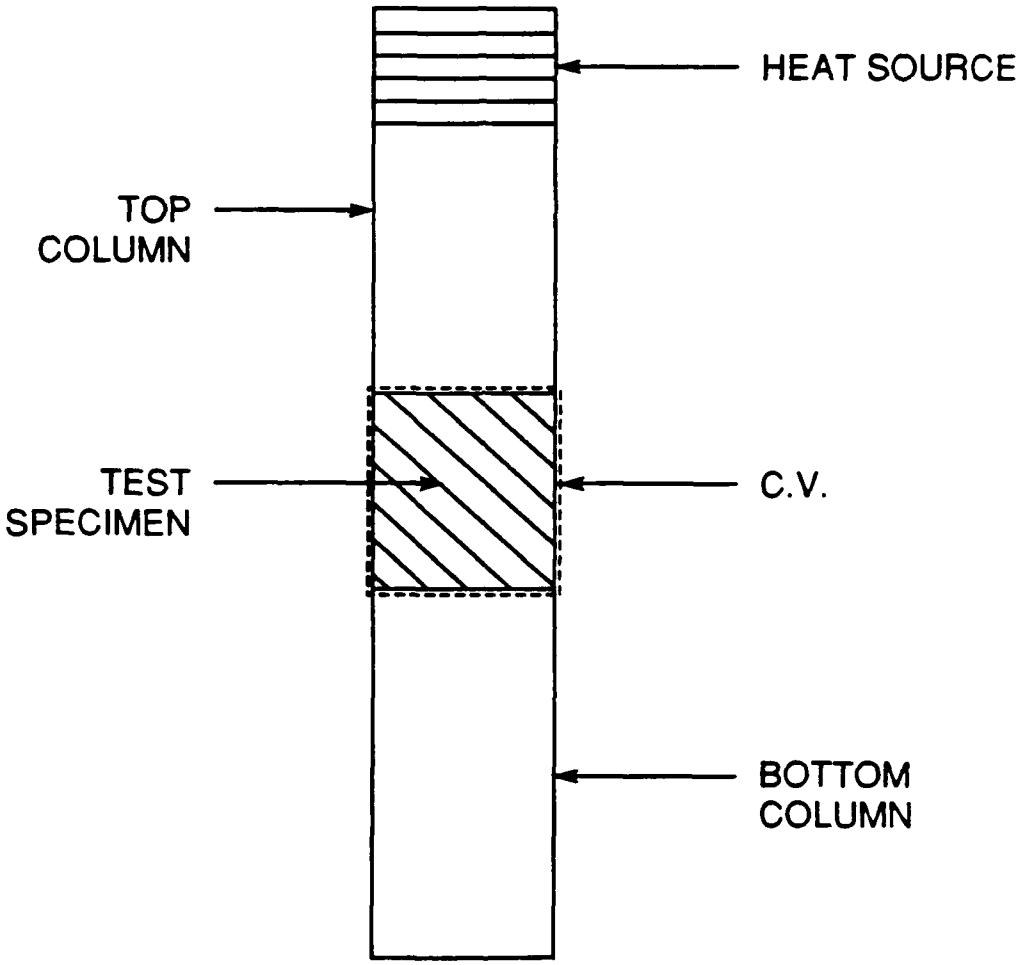

Fig. 11 Basic apparatus used for the Saran Carbon experiment

2.5 Saran Carbon Experimental Apparatus

The Saran Carbon experimental apparatus, which can be seen in Figure 12, is suitable for thermal conductivity measurements on rigid rod samples in the temperature range between -20°C and 200°C. The dimensions of the apparatus are as indicated in the figure. The apparatus was composed of a top aluminum column with a heater attached, a spacer made of insulation, a load plate with a support structure, a bottom stainless-steel column, and a stainless steel reference plate. The carbon was sandwiched between the top and bottom columns. The load plate was used to insure good surface contact between the columns and the carbon by providing an axial load onto the column as the plate was bolted to the support structure. The insulation was used to minimize heat transfer into the load plate. A 240-W, 120 Volt coil heater was wrapped around the top aluminum column to provide the needed heat source. A highly reflective radiation shield was installed around the column to reduce radial heat losses due to radiation heat transfer.

Ten insulated Chromel-Alumel thermocouples, 0.099 cm diameter, were installed in holes drilled into the centerline position. All of the thermocouples were held into place by a highly conductive epoxy (OMEGABOND 200). Using the known values of the temperatures and distances between the thermocouple locations in the stainless steel

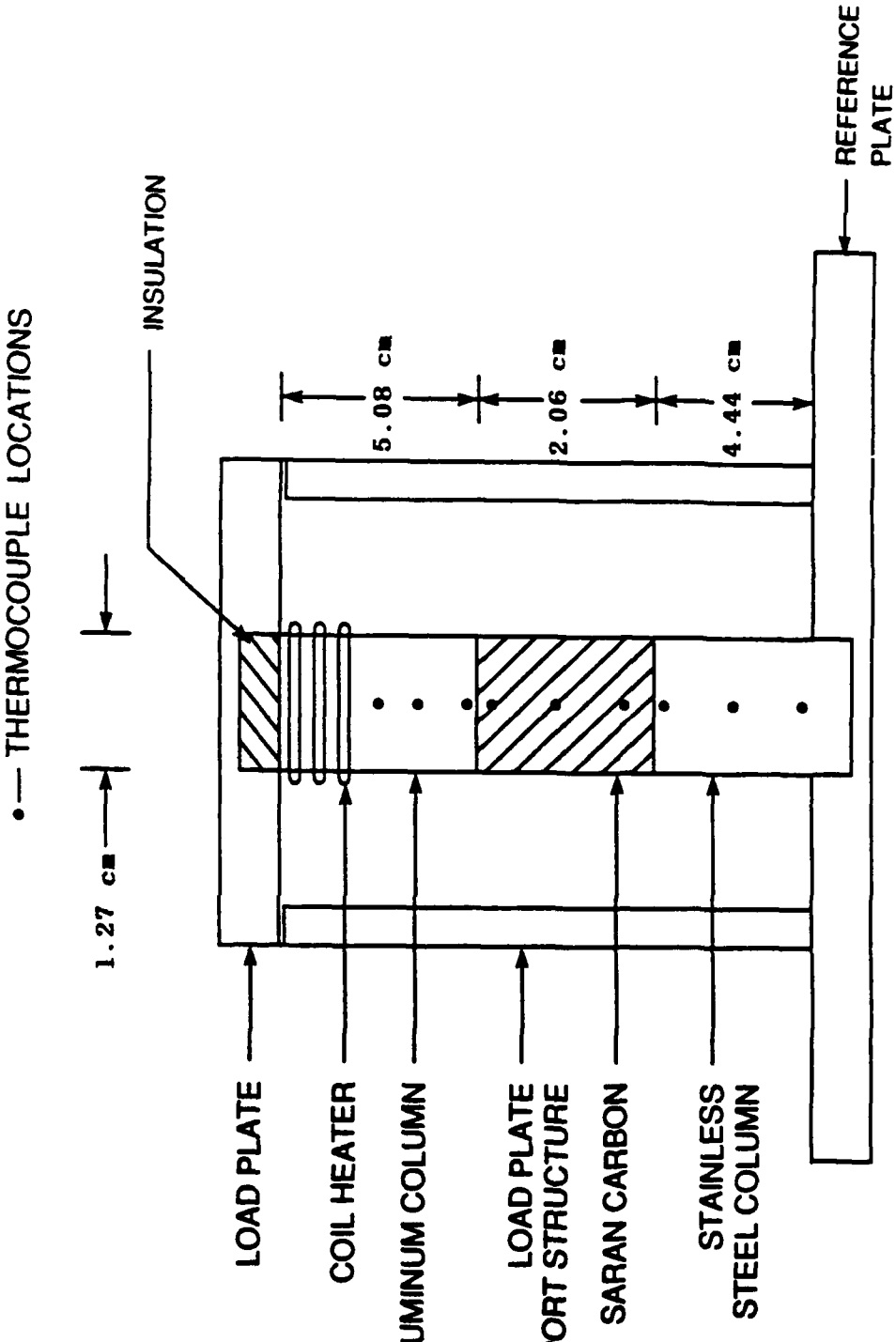

Fig. 12 Saran Carbon experimental apparatus

column, as well as the thermal conductivity of stainless steel, the energy transfer, Q, into the stainless steel column could be determined. With Q as a known quantity equation (1) could be used to solve for the thermal conductivity of the Saran Carbon.

The temperature of the apparatus was controlled by one Digi-Sense proportional temperature controller as discussed in section 2.2. One of the installed thermocouples provided the needed temperature sensor for the controller. The temperature of the reference plate was controlled by either the fluidized bed or a constant temperature bath, depending on the desired temperature of the plate. The constant temperature fluidized bed provided control between 50°C and 200°C, and the constant temperature bath provided control between -20°C and 49°C.

The thermal conductivity of the carbon was determined in a vacuum environment. This was necessary to eliminate conduction losses to the surrounding air and also to eliminate the effects of any interstitial fluids on the thermal conductivity. For the Saran Carbon powder (2 μm in diameter) a vacuum level of 1×10^{-3} torr or better was necessary to eliminate gaseous conduction as discussed previously in section 2.2. The reference plate was bolted to the vacuum chamber. The thermocouple and heater leads were passed from the inside of the chamber to an outside switchbox as discussed previously in section 2.2.

2.6 Experimental Procedure

The Saran Carbon test specimen was formed, by JPL, into an approximately 0.127 cm OD rod by compressing the carbon powder into a die assembly to a density of 1.135 grams/cm^3, and a porosity of 47.2 percent. After compression, the rod was removed from the die assembly and cut to a length of 2.06 cm. The test column was fully assembled and bolted, after attaching the inner leads to the vacuum feedthrough system and installing the radiation shield, to the vacuum chamber.

After assembling the apparatus, the vacuum chamber was immersed into the fluidized bed or the constant temperature bath as mentioned before. The vacuum system was turned on and allowed to reach a constant level of vacuum inside the chamber. For all of the experimental runs a vacuum of better than 1×10^{-4} torr was achieved. After outgassing, all temperature controllers were set to the desired ΔT across the carbon specimen. Data was then taken at 30 minute intervals until steady-state conditions were insured in the same manner as discussed in section 2.3. The data consisted of the temperatures at each thermocouple location, vacuum level inside the chamber, bath temperature, and power setting of the heater. The ΔT across the carbon was then adjusted to a different setting and the procedure was repeated once again. The uncertainties in the values of the

thermal conductivity ranged from ± 5.43 percent to ± 12.94 percent as given in Appendix D. For approximately eighty percent of the runs the uncertainty in the values of the thermal conductivity was less than 8.17 percent.

CHAPTER 3

RESULTS AND DISCUSSION

Table 1 shows a summary of the test conditions and results for the PCO experiment. In this case, the mean temperature (T_{mean}) is the arithmetic mean between the hot and cold plate temperatures. The thermal conductivity values were calculated from equation (1) as mentioned in section 2.2.

Table 1 PCO experimental conditions and results

Run #	T_{mean}, °C	T_h, °C	T_c, °C	Pulse, count	Δt, secs	k, W/m°C
1	312.57	326.15	299.00	7005.0	5212.40	0.1471
2	323.40	335.20	311.60	5830.0	5340.32	0.1378
3	362.00	375.50	348.50	9274.0	5232.58	0.1957
4	410.15	422.90	397.40	12681.0	5099.58	0.2867
5	457.60	470.30	444.90	18200.0	4907.68	0.4207
6	507.65	519.65	495.65	23020.0	5335.63	0.5211
7	556.43	568.20	544.65	27990.0	5394.38	0.6389
8	591.95	614.60	569.30	49466.0	4080.28	0.7624

Figure 13 illustrates the results of the PCO experiment. As shown, the thermal conductivity of the PCO has a strong temperature dependency. The line in the figure was obtained from the following equation

$$k = -0.00013 - 0.319659E\text{-}3T_{mean} + 0.160629E\text{-}8T_{mean}^3 \quad (2)$$

which was a least-squares-error fit of the data with T_{mean} in Kelvin. The error sum of squares is 0.14 percent, indicating a very good fit through the points. The first

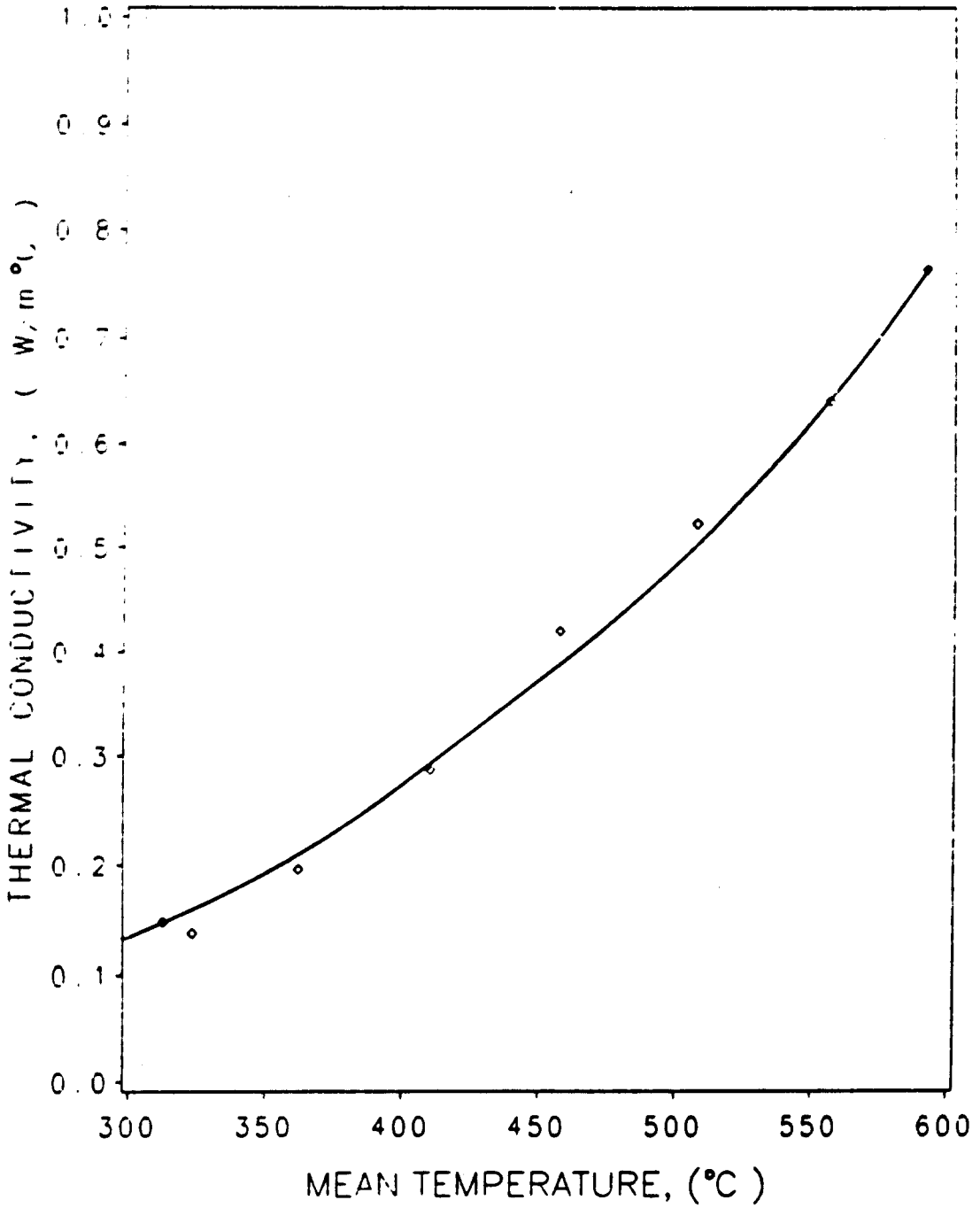

Fig. 13 Thermal conductivity of the PCO

BEST
AVAILABLE COPY

two terms on the right-hand side allows for a linear temperature variation. The cubic term is included to account for possible radiation contribution to the thermal conductivity. The cubic term arises from the basic definition of the total thermal conductivity of a porous material.[8] In this case, it's magnitude is comparable to the other terms in the equation, indicating an appreciable radiation contribution to the thermal conductivity.

Equation (2) was used to calculate the thermal conductivity at each mean temperature, and then these values were compared with the experimental results as shown in Table 2. As indicated in the table, the greatest difference between the correlation and the experimentally obtained values is 8.68 percent, with 75 percent of the results within 5.84 percent or less.

Table 2 Comparison of calculated values from equation (2) with experimentally obtained values of the PCO

T_{mean}, °C	Calculated k, W/m°C	Experimental k, W/m°C	Difference, percent
312.57	0.1352	0.1471	8.68
323.40	0.1499	0.1378	8.65
362.00	0.2081	0.1957	5.84
410.15	0.2935	0.2867	2.22
457.60	0.3927	0.4207	6.94
507.65	0.5145	0.5211	1.26
556.43	0.6512	0.6389	1.87
591.95	0.7626	0.7624	0.85

Table 3 gives a summary of the test conditions and results for the Saran Carbon experiment. In this experiment, the mean temperature is the arithmetic mean

between thermocouples # 4 and # 6 located in the carbon rod (see Appendix F). Equation (1) was used to obtain the thermal conductivity values shown in the table. This was accomplished in the following manner. First, a plot of temperature against thermocouple location was generated for the stainless steel column. Then, a straight temperature distribution line was fit through the three data points and was used to determine Q through the stainless steel column. To satisfy energy balance, heat transfer through the carbon rod must have the same Q. Similarly, a straight line was fit through the three temperature data points for the carbon rod. The thermal conductivity of the carbon was solved for by equating $Q/k_{ss}A$ to the slope of the straight line.

Table 3 Saran Carbon experimental conditions and results

Run, #	T_{mean}, °C	T_h, °C	T_c, °C	k, W/m°C
1	2.89	8.20	-2.40	0.785
2	33.54	46.90	20.17	0.702
3	66.22	87.81	44.63	0.709
4	77.58	85.23	69.93	0.883
5	78.64	86.28	70.98	0.878
6	115.77	130.12	101.42	0.976
7	133.00	150.41	115.60	1.040
8	133.10	152.21	114.00	1.077
9	133.83	141.96	125.70	1.082
10	142.16	160.72	123.60	1.100
11	142.80	162.37	123.23	1.106
12	166.72	189.99	143.44	1.142
13	193.70	211.96	175.42	1.166

Figure 14 shows the experimental thermal conductivity plotted against mean temperature. The data was obtained over the temperature range used in the Saran Carbon

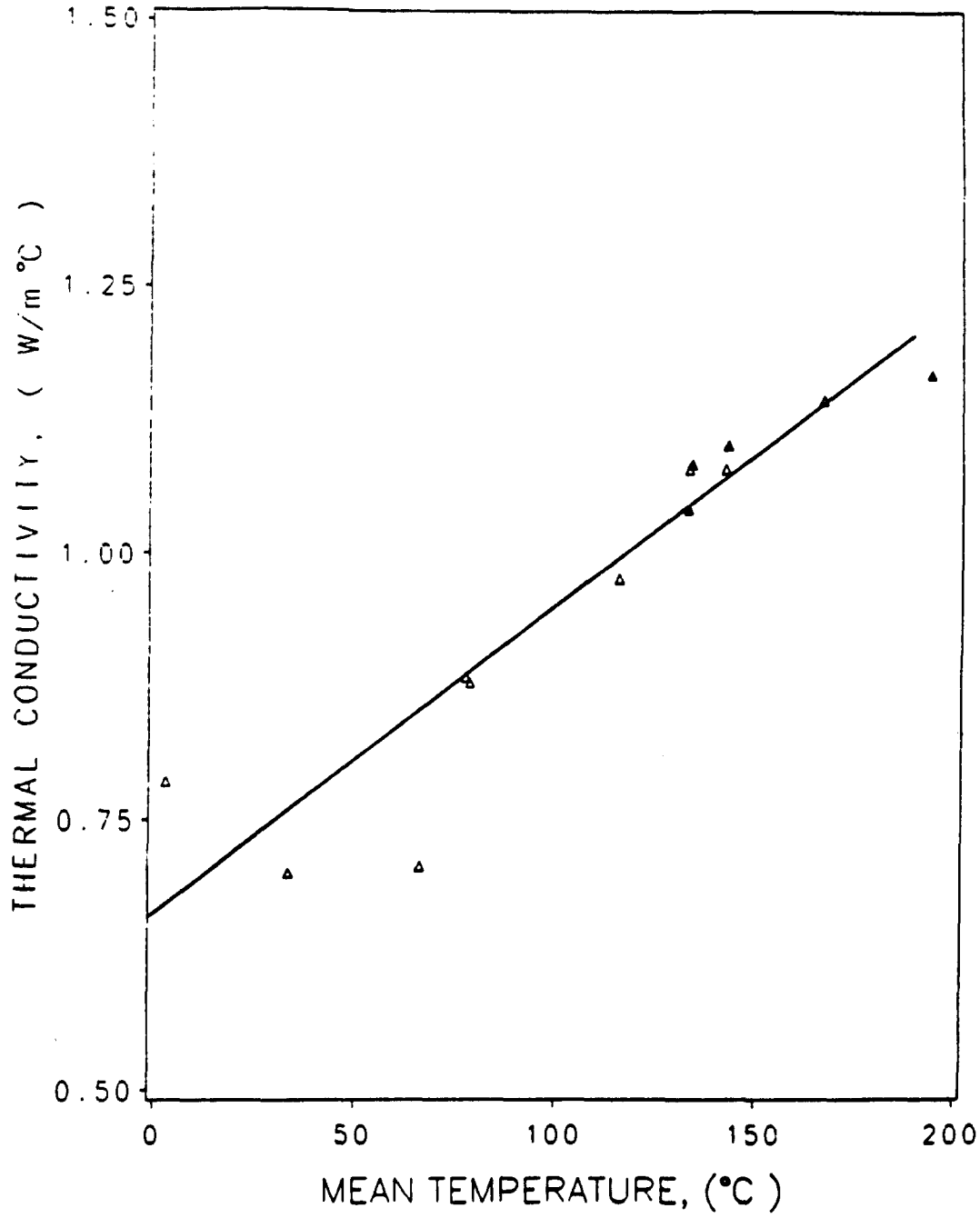

Fig. 14 Thermal conductivity of the Saran Carbon

adsorption compressors. The solid symbols represent the data obtained using the sand bed and the open symbols represent the data obtained using the constant temperature bath. As shown in the figure, the thermal conductivity increases with a corresponding increase in the mean temperature. The following equation

$$k = 0.20359 + 0.154475E\text{-}2T_{mean} + 0.303628E\text{-}9T_{mean}^{3} \quad (3)$$

was again obtained through a least-squares-error fit of the data with T_{mean} in Kelvin. For this fit, the error sum of squares is 4.28 percent. In this case, the contribution of radiation is negligible since the cubic term is very small compared to the first two terms, even for the data point with the highest mean temperature. In fact, a fit with a linear function yielded

$$k = -0.10115 + 0.280980E\text{-}2T_{mean} \quad (4)$$

with 4.41 percent as the error sum of squares and T_{mean} in Kelvin. The line in Figure 14 was obtained from equation (3). It is clear that a linear variation is sufficient to allow for the temperature dependency.

Equation (4) was used to calculate the thermal conductivity at each mean temperature value, and then these values were compared with the experimental results as shown in Table 4. As indicated in the table, the greatest difference between the calculated values and the

experimentally obtained values is 16.78 percent, with 84.6 percent of the results within 7.64 percent or less.

Table 4 Comparison of calculated values from equation (4) with experimentally obtained values of the Saran Carbon

T_{mean}, °C	Calculated k, W/m°C	Experimental k, W/m°C	Difference, percent
2.89	0.6740	0.7850	16.47
33.54	0.7601	0.7020	7.64
66.22	0.8520	0.7090	16.78
77.58	0.8840	0.8830	0.11
78.64	0.8870	0.8780	1.01
115.77	0.9912	0.9760	1.54
133.00	1.0396	1.0400	0.04
133.10	1.0399	1.0770	3.56
133.83	1.0419	1.0820	3.85
142.16	1.0654	1.1000	3.24
142.80	1.0672	1.1060	3.63
166.72	1.1344	1.1420	0.67
193.70	1.2102	1.1660	3.65

The thermal conductivity of the Saran Carbon is further compared to the thermal conductivity of porous carbon, which is assumed to be given by the following relationship

$$k = \varepsilon k_l + (1-\varepsilon)k_s \qquad (5)$$

where ε is the porosity of the porous carbon, which is assumed to be the same as the Saran Carbon, k_l is the thermal conductivity of the interstitial fluid (in this experiment $k_l = 0$), and k_s is the thermal conductivity of solid carbon. Table 5 shows the comparison between the Saran Carbon and porous carbon at different mean temperature values with $\varepsilon = 47.2$ percent. The largest difference is

24.70 percent, with 84.6 percent of the experimental results falling within 9.88 percent of each other.

Table 5 Comparison of Saran Carbon with solid carbon

T_{mean}, °C	T_h, °C	T_c, °C	k, W/m°C	k_s, W/m°C	$(1-\varepsilon)k_s$, W/m°C
2.89	8.20	-2.40	0.785	1.449	0.765
33.54	46.90	20.17	0.702	1.558	0.822
66.22	87.81	44.63	0.709	1.674	0.883
77.58	85.23	69.93	0.883	1.715	0.905
78.64	86.28	70.98	0.878	1.718	0.907
115.77	130.12	101.42	0.976	1.850	0.976
133.00	150.41	115.60	1.040	1.900	1.002
133.10	152.21	114.00	1.077	1.901	1.002
133.83	141.96	125.70	1.082	1.902	1.003
142.16	160.72	123.60	1.100	1.913	1.010
142.80	162.37	123.23	1.106	1.915	1.010
166.72	189.99	143.44	1.142	1.950	1.029
193.70	211.96	175.42	1.166	1.990	1.050

CHAPTER 4

CONCLUSIONS

Numerical studies are being conducted by Sathe and Tong to better understand the heat and fluid flow characterics inside porous adsorbents[4] used in laboratory adsorption compressors. These compressors use Praseodymium-Cerium-Oxide (PCO) and Saran Carbon as the adsorbents. At the present time, these studies use an assumed value for the thermal conductivity of the PCO and Saran Carbon due to lack of data. It was the objective of the present investigation to experimentally obtain values for the thermal conductivity of both materials.

Since the porous materials came in different forms, the PCO in a powder and the Saran Carbon in a rigid rod, two types of test sections were needed for the thermal conductivity measurements. A circular guarded-hot-plate apparatus was designed and built for the PCO experiment, while a column apparatus was used for the Saran Carbon. Both test sections simulate steady-state, one-dimensional heat transfer across the material of interest.

Results of the thermal conductivity measurements suggest a strong temperature dependency for both materials. A least-squared-error fit program was used to fit a line through the PCO and Saran Carbon data points. Comparison between the calculated values from equation (2) and the

experimentally obtained values of the PCO thermal conductivity indicates that 75 percent of the data is within 5.84 percent or less of the line in Figure 13. Comparison between the Saran Carbon and porous carbon shows the greatest difference as 24.7 percent, with 84.6 percent of the experimental results within 9.88 percent of the porous values (see Table 5).

Radiation effects significantly contributed to the thermal conductivity measurements of the PCO, while showing a negligible contribution to the thermal conductivity of the Saran Carbon.

REFERENCES

[1]Bard, S., "Development of an 80-120 K Charcoal-Nitrogen Adsorption Cryocooler," Proceedings of the Fourth International Cryocooler Conference, Easton, MD, Sept., 1986.

[2]Jones, J. A., "Sorption Refrigeration Comparision Study," Proceedings of the Eleventh International Cryogenic Engineering Conference, Berlin-West, April, 1986.

[3]Bard, S., "Improving Adsorption Cryocoolers by Multistage Compression and Reducing Void Volume," *Cryogenics*, Vol. 26, June 1986, pp. 450.

[4]Sathe, S. B., and Tong, T. W., "Transient Heat and Fluid Flow in Porous Annuli," Proceedings of the 27th Aerospace Sciences Meeting, Reno, NV, Jan., 1989.

[5]ASTM, 1968a., Standard method of test for thermal conductivity of materials by means of the guarded hot plate, ASTM, C 177-63., Philadelphia, Pa., 1968.

[6]Hemminger, W., and Jugel, R., "A Guarded Hot-Plate Apparatus for Thermal Conductivity Measurements over the Temperature Range -75 to 200°C," *International Journal of Thermophysics*, Vol. 6, No. 5, 1985, pp. 483-498.

[7]Patankar, S., *Numerical Heat Transfer and Fluid Flow*, Hemisphere Publishing Corporation, New York, 1980.

[8]Reiss, H., "Evacuated Load-Bearing Powder Insulation for High Temperature Applications," *Journal of Energy*, Vol. 7, April 1983, pp. 152-159.

[9]Peterson, G. P., Fletcher, L. S., "Effective Thermal Conductivity of Sintered Heat Pipe Wicks," *Journal of Thermophysics*, Vol. 1, No. 4, Oct. 1987, pp. 343-347.

[10]Clausing, A. M., and Chao, B. T., "Thermal Contact Resistance in a Vacuum Environment," *Journal of Heat Transfer*, May 1965, pp. 243-251.

[11]Miller, R. G., and Fletcher, L. S., "Thermal Contact Resistance of Porous Metallic Materials in a Vacuum Environment," *Progess in Astronautics and Aeronautics Thermophysics and Spacecraft Thermal Control*, Vol. 35, June 1974, pp. 321-324.

APPENDIX A

Power Pulse Meter

The power pulse meter is a device that counts the number of pulses delivered to the inner heater in a certain time interval. The meter senses the half wavelength of an a.c. power pulse. When full power is applied the meter counts 120 pulses per second, because there are 120 half wavelengths in a 60 Hz power supply.

For example, consider the following case. The resistance (R) of the inner heater is 116.58 Ω. At full power the r.m.s. voltage drop (Ve) across the inner heater was 117.05V. Thus,

Full power = Ve^2/R = 117.52W.

Now, with 2448 power pulses supplied to the inner heater in a time interval (Δt) of 392.72 secs we have:

Average power = Full power × 2448/(120 × 392.72) = 6.1W

Therefore, average power corresponds to Q in equation (1).

APPENDIX B

Feedthrough Calibration

In both experiments a feedthrough system was used to collect mv reading from various thermocouples located inside the vacuum chamber. To verify if any error would be introduced by the feedthrough system two thermocouple circuits for each experiment were built. One circuit had the feedthrough system installed (WFT) while the other did not. Data was taken for each circuit across a range of temperatures (see Table 6) and then the circuit with the feedthrough was calibrated against the circuit without the feedthrough.

Table 6 Calibration of thermocouples

Temp, °C	Saran Carbon WFT, mv	Saran Carbon Other, mv	PCO WFT, mv	PCO Other, mv
80	3.274	3.268	3.283	3.277
100	4.099	4.096	4.105	4.103
120	4.923	4.921	4.931	4.929
140	5.740	5.744	5.749	5.746
160	6.586	6.581	6.572	6.574
200	8.230	8.232	8.219	8.217
230	9.468	9.462	9.425	9.418
270	11.096	11.089	11.078	11.086
310	12.753	12.748	12.718	12.723
350	14.385	14.380	14.350	14.354
400	16.426	16.423	16.398	16.399
450	18.463	18.460	18.438	18.440
500	20.494	20.491	20.482	20.485

APPENDIX C

Error Analysis for the PCO

From equation (1) we have:

$$k = Q\Delta x/A\Delta T$$

but $Q = Ve^2(count)/120R\Delta t$

where count is the number of pulses delivered to the inner heater in a time interval (Δt). and Ve^2, R are defined in Appendix A. So k is now:

$$k = (Ve^2 count\Delta x/120R\Delta t)/A\Delta T$$

The root mean square error is given by:

$$\Delta k/k = \{(2\Delta Ve/\Delta Ve)^2 + (\Delta count/count)^2 + (\Delta R/R)^2 + (\Delta(\Delta t)/\Delta t)^2 + (\Delta(\Delta x)/\Delta x)^2 + (\Delta A/A)^2 + (\Delta T_h/\Delta T)^2 + (\Delta T_c/\Delta T)^2\}^{1/2}$$

For example consider the following case:

ΔVe	= 1.57V	Ve	= 117.05V
$\Delta count$	= 0.5	count	= 2448
ΔR	= 0.005 Ω	R	= 116.58 Ω
$\Delta(\Delta t)$	= 0.005 secs	Δt	= 392.72 secs
$\Delta(\Delta x)$	= 1.016E-4 m	Δx	= 6.35E-3 m
ΔA	= 1.805E-6 m	A	= 6.43E-3 m
ΔT_h	= 0.2 °C	ΔT	= 25 °C
ΔT_c	= 0.2 °C		

The error in the resistance, and voltage is from the FLUKE 8842A multimeter used in the experiment.

Substituting the above values in the root mean square error equation yields:

$\Delta k/k$ = 0.05044 i.e. an uncertainty of ± 5.044 percent.

APPENDIX D

Error Analysis for the Saran Carbon

Again, from equation (1) we have:

$$k = Q\Delta x_{car}/A\Delta T_{car}$$

but for this case,

$$Q = k_{ss}A\Delta T_{ss}/\Delta x_{ss}$$

where k_{ss} is the thermal conductivity of the stainless steel column, ΔT_{ss} is the temperature difference ($T_3 - T_1$) in the stainless steel column, Δx_{ss} is the distance between thermocouple locations in the stainless steel column, and ΔT_{car} is the temperature difference ($T_6 - T_4$) in the Saran Carbon. So k is now:

$$k = (k_{ss}A\Delta T_{ss}/\Delta x_{ss})\Delta x_{car}/A\Delta T_{car}$$

The root mean square error is given by:

$$\Delta k/k = \{(\Delta k_{ss}/k_{ss})^2 + (2(\Delta A/A)^2) + (\Delta T_h/\Delta T_{ss})^2 + (\Delta T_c/\Delta T_{ss})^2 + (\Delta(\Delta x_{ss})/\Delta x_{ss})^2 + (\Delta(\Delta x)/\Delta x_{car})^2 + (\Delta T_h/\Delta T_{car})^2 + (\Delta T_c/\Delta T_{car})^2\}^{1/2}$$

Consider the following example:

Δk_{ss}	= 0.800 W/m°C	k_{ss}	= 16.013 W/m°C
ΔA	= 2.49E-7 m	A	= 1.224E-4 m
ΔT_h	= ΔT_c = 0.2 °C	ΔT_{ss}	= 17.027 °C
$\Delta(\Delta x_{ss})$	= 1.27E-6 m	Δxss	= 4.048E-2 m
$\Delta(\Delta x)$	= 1.27E-6 m	Δx_{car}	= 9.855E-3 m
ΔT_{car}	= 38.145 °C		

where Δx_{car} is the distance between thermocouples in the Saran Carbon.

Substituting the above values in the root mean square error equation yields:

$\Delta k/k$ = 0.05328 i.e. an uncertainty of 5.328 percent.

APPENDIX E

PCO Experimental Data

Table 7 PCO experimental data for run # 1

Thermocouple, #	e.m.f., mv	°C
1	13.299	326.103
3	13.306	326.296
4	12.450	305.580
6	13.208	323.908
7	13.230	324.439
9	12.180	299.033
10	12.173	298.864

Thermocouple numbering code as per location:
1 - 3 --- inner copper plate
4 - 5 --- outer copper plate
6 - 8 --- top copper plate
9 - 10 -- reference plate
note : thermocouples # 2,5,8 were used to regulate controllers

inner heater controller temperature = 325.2 °C
guard heater controller temperature = 307.2 °C
top heater controller temperature = 337.1 °C
bed controller temperature = 305.0 °C
resistance of inner heater = 84.20 Ω
count = 7005
Δt = 5212.41 secs
vacuum = 9E-5 torr
r.m.s. voltage drop across inner heater = 122.35 volts
Δx = 6.35E-3 m
area perpendicular to heat transfer = 3.167E-3 m^2

Table 8 PCO experimental data for run # 3

Thermocouple, #	e.m.f., mv	°C
1	15.332	374.868
3	15.348	375.250
4	14.380	352.099
6	15.235	372.553
7	15.268	373.341
9	14.244	348.837
10	14.218	348.213

inner heater controller temperature = 376.0 °C
guard heater controller temperature = 356.3 °C
top heater controller temperatue = 388.3 °C
bed controller temperature = 355.0 °C
resistance of inner heater = 85.47 Ω
count = 9274
Δt = 5232.58 secs
vacuum = 1.5E-4 torr
r.m.s. voltage drop
across inner heater = 122.63 volts

Table 9 PCO experimental data for run # 4

Thermocouple, #	e.m.f., mv	°C
1	17.343	422.615
3	17.365	422.135
4	16.280	397.432
6	17.318	422.024
7	17.321	422.095
9	16.292	397.717
10	16.268	397.147

inner heater controller temperature = 425.6 °C
guard heater controller temperature = 401.5 °C
top heater controller temperature = 441.4 °C
bed controller temperature = 405.0 °C
resistance of inner heater = 85.47 Ω
count = 12681
Δt = 5099.58 secs
vacuum = 1.4E-4 torr
r.m.s. voltage drop
across inner heater = 121.92 volts

APPENDIX F

Saran Carbon Experimental Data

Table 10 Saran Carbon experimental data for run # 1

Thermocouple, #	e.m.f., mv	°C
1	-0.644	-15.300
2	-0.590	-14.000
3	-0.543	-12.869
4	-0.109	-2.405
5	0.108	2.836
6	0.330	8.204
7	0.901	22.043
8	0.916	22.407
9	0.920	22.505

Thermocouple numbering code as per location:
1 - 3 --- bottom stainless steel column
4 - 6 --- Saran Carbon sample
7 - 9 --- top aluminum column
note : thermocouple # 10 was used to regulate controller. Thermophysical properties of stainless steel were evaluated using the temperature at thermocouple location # 2

distance between thermocouple # 1 and # 3 = 4.0481E-2 m
distance between thermocouple # 4 and # 6 = 9.8552E-3 m
area perpendicular to heat transfer = 1.2240E-4 m^2
variac setting = 5
constant temperature bath = -22.0 °C
controller temperature = 22.5 °C

Table 11 Saran Carbon experimental data for run # 4

Thermocouple, #	e.m.f., mv	°C
1	1.030	25.176
2	1.111	27.144
3	1.182	28.870
4	2.863	69.928
5	3.150	76.971
6	3.486	85.227
7	6.406	157.281
8	6.338	155.600
9	6.442	158.195

variac setting = 16

constant temperature bath = 16.0 °C
controller temperature = 158.4 °C

REFERENCES

[1]Bard, S., "Development of an 80-120 K Charcoal-Nitrogen Adsorption Cryocooler," Proceedings of the Fourth International Cryocooler Conference, Easton, MD, Sept., 1986.

[2]Jones, J. A., "Sorption Refrigeration Comparision Study," Proceedings of the Eleventh International Cryogenic Engineering Conference, Berlin-West, April, 1986.

[3]Bard, S., "Improving Adsorption Cryocoolers by Multistage Compression and Reducing Void Volume," *Cryogenics*, Vol. 26, June 1986, pp. 450.

[4]Sathe, S. B., and Tong, T. W., "Transient Heat and Fluid Flow in Porous Annuli," Proceedings of the 27th Aerospace Sciences Meeting, Reno, NV, Jan., 1989.

[5]ASTM, 1968a., Standard method of test for thermal conductivity of materials by means of the guarded hot plate, ASTM, C 177-63., Philadelphia, Pa., 1968.

[6]Hemminger, W., and Jugel, R., "A Guarded Hot-Plate Apparatus for Thermal Conductivity Measurements over the Temperature Range -75 to 200°C," *International Journal of Thermophysics*, Vol. 6, No. 5, 1985, pp. 483-498.

[7]Patankar, S., *Numerical Heat Transfer and Fluid Flow*, Hemisphere Publishing Corporation, New York, 1980.

[8]Reiss, H., "Evacuated Load-Bearing Powder Insulation for High Temperature Applications," *Journal of Energy*, Vol. 7, April 1983, pp. 152-159.

[9]Peterson, G. P., Fletcher, L. S., "Effective Thermal Conductivity of Sintered Heat Pipe Wicks," *Journal of Thermophysics*, Vol. 1, No. 4, Oct. 1987, pp. 343-347.

[10]Clausing, A. M., and Chao, B. T., "Thermal Contact Resistance in a Vacuum Environment," *Journal of Heat Transfer*, May 1965, pp. 243-251.

[11]Miller, R. G., and Fletcher, L. S., "Thermal Contact Resistance of Porous Metallic Materials in a Vacuum Environment," *Progess in Astronautics and Aeronautics Thermophysics and Spacecraft Thermal Control*, Vol. 35, June 1974, pp. 321-324.

REFERENCES

[1]Bard, S., "Development of an 80-120 K Charcoal-Nitrogen Adsorption Cryocooler," Proceedings of the Fourth International Cryocooler Conference, Easton, MD, Sept., 1986.

[2]Jones, J. A., "Sorption Refrigeration Comparision Study," Proceedings of the Eleventh International Cryogenic Engineering Conference, Berlin-West, April, 1986.

[3]Bard, S., "Improving Adsorption Cryocoolers by Multistage Compression and Reducing Void Volume," *Cryogenics*, Vol. 26, June 1986, pp. 450.

[4]Sathe, S. B., and Tong, T. W., "Transient Heat and Fluid Flow in Porous Annuli," Proceedings of the 27th Aerospace Sciences Meeting, Reno, NV, Jan., 1989.

[5]ASTM, 1968a., Standard method of test for thermal conductivity of materials by means of the guarded hot plate, ASTM, C 177-63., Philadelphia, Pa., 1968.

[6]Hemminger, W., and Jugel, R., "A Guarded Hot-Plate Apparatus for Thermal Conductivity Measurements over the Temperature Range -75 to 200°C," *International Journal of Thermophysics*, Vol. 6, No. 5, 1985, pp. 483-498.

[7]Patankar, S., *Numerical Heat Transfer and Fluid Flow*, Hemisphere Publishing Corporation, New York, 1980.

[8]Reiss, H., "Evacuated Load-Bearing Powder Insulation for High Temperature Applications," *Journal of Energy*, Vol. 7, April 1983, pp. 152-159.

[9]Peterson, G. P., Fletcher, L. S., "Effective Thermal Conductivity of Sintered Heat Pipe Wicks," *Journal of Thermophysics*, Vol. 1, No. 4, Oct. 1987, pp. 343-347.

[10]Clausing, A. M., and Chao, B. T., "Thermal Contact Resistance in a Vacuum Environment," *Journal of Heat Transfer*, May 1965, pp. 243-251.

[11]Miller, R. G., and Fletcher, L. S., "Thermal Contact Resistance of Porous Metallic Materials in a Vacuum Environment," *Progess in Astronautics and Aeronautics Thermophysics and Spacecraft Thermal Control*, Vol. 35, June 1974, pp. 321-324.